Novel Microporous Europium and Terbium Silicates

ARTICLE *in* JOURNAL OF THE AMERICAN CHEMICAL SOCIETY · JUNE 2001

Impact Factor: 12.11 · DOI: 10.1021/ja010244z · Source: PubMed

Novel Microporous Europium and Terbium Silicates

Duarte Ananias,[†] Artur Ferreira,[‡] João Rocha,[†,*] Paula Ferreira,[†] José P. Rainho,[†,§] Cláudia Morais,[†] and Luís D. Carlos[§]

Contribution from the Department of Chemistry, ESTGA, and Department of Physics, University of Aveiro, 3810-193 Aveiro, Portugal, ESTGA, University of Aveiro, 3810-193 Aveiro, Portugal

Received January 29, 2001

Abstract: The synthesis and structural characterization of the first examples of microporous europium(III) and terbium(III) silicates ($Na_4K_2X_2Si_{16}O_{38}\cdot 10H_2O$, X = Eu, Tb) are reported. The structure of these solids was solved by powder X-ray diffraction ab initio (direct) methods and further characterized by chemical analysis (EDS), thermogravimetric analysis (TGA), scanning electron microscopy (SEM), ^{23}Na and ^{29}Si magic-angle spinning (MAS) NMR, and luminescence spectroscopy. Both materials display interesting photoluminescence properties and present potential for applications in optoelectronics. This work illustrates the possibility of combining in a given silicate microporosity and optical activity.

Introduction

Zeolites are crystalline, hydrated aluminosilicates with open three-dimensional structures built of $[SiO_4]^{4-}$ and $[AlO_4]^{5-}$ tetrahedra linked to each other by sharing all the oxygens to form regular intracrystalline cavities and channels of molecular dimensions. These materials are of considerable technological importance as shape-selective catalysts, ion-exchange solids, and molecular sieves. Many other materials with zeolite-type structures, particularly porous aluminophosphates and derivatives, are known, all of which contain tetrahedrally coordinated metal atoms.[1] Recently, much research has been carried out aimed at preparing inorganic microporous framework solids containing atoms in different coordination geometries.[2] One such family of materials is of considerable interest, microporous titanosilicates (known as ETS materials) and derivatives containing Ti^{4+} usually in octahedral coordination.[3,4] We have been interested in the chemistry of novel mixed octahedral−tetrahedral microporous framework silicates for the past 7 years.[4,5]

The synthesis and characterization of AV-1, a sodium yttrium silicate possessing the structure of the mineral montregianite, has been reported.[6,7] Montregianite is a very rare hydrous sodium potassium yttrium silicate ($Na_4K_2Y_2Si_{16}O_{38}\cdot 10H_2O$) from Mont St. Hilaire, Québec, Canada, where it occurs in miarolitic cavities and as thermally metamorphosed inclusions and rheomorphic breccias in nepheline syenite.[8] In nature, montregianite usually occurs with substitution of some yttrium by cerium. Recently, the synthesis of a purely cereous form of AV-1 has been reported.[9]

Lanthanide Eu(III) and Tb(III) complexes present a great potential for photonic applications, as light sources, X-ray phosphors and scintillator display devices, detector systems, light-emitting diodes, and solid-state lasers.[10−13] Moreover, the recent years have witnessed a renaissance in lanthanide chemistry, driven by the need for tailored long-lived Eu(III) and Tb(III) complexes for use in magnetic resonance imaging, targeted radiotherapy, and as alternatives for radioimmuno assay probes.[14] The Eu(III) 610 nm luminescence, for instance, is widely used in red phosphors for the lighting industry and in light-emitting diodes and solid-state laser devices.[10] Furthermore, the Eu(III) and Tb(III) ions have been used as luminescent probes to study the symmetry and the local environment of the lanthanide species in a variety of compounds such as glasses, polymeric materials, biological macromolecules, etc.[12,13] Spectroscopic studies have also been carried out on microporous rare-earth dicarboxylates and europium hybrid compounds.[15,16]

Our main aim with this work was to explore the possibility of combining, in a given silicate, microporosity and optical activity. Thus, here we wish to report the synthesis and characterization of Eu(III) and Tb(III) silicates possessing a

* Address correspondence to this author. Fax: +351 234 370084. Phone: +351 234 370730. E-mail: ROCHA@DQ.UA.PT.

[†] Department of Chemistry.

[‡] ESTGA.

[§] Department of Physics.

(1) Szostak, R. *Molecular Sieves*; Van Nostrand Reinhold: New York, 1989.

(2) Cheetham, A. K.; Ferey, G.; Loiseau, T. *Angew. Chem., Int. Ed.* **1999**, *38*, 3268.

(3) Kuznicki, S. M. U.S. Patent 485.320.2, 1989.

(4) Anderson, M. W.; Terasaki, O.; Ohsuma, T.; Phillippou, A.; Mackay, S. P.; Ferreira, A.; Rocha, J.; Lidin, S. *Nature* **1994**, *367*, 347.

(5) Rocha, J.; Anderson, M. W. *Eur. J. Inorg. Chem.* **2000**, 801.

(6) Rocha, J.; Ferreira, P.; Lin, Z.; Brandão, P.; Ferreira, A.; Pedrosa de Jesus, J. D. *Chem. Commun.* **1997**, 2103.

(7) Rocha, J.; Ferreira, P.; Lin, Z.; Brandão, P.; Ferreira, A.; Pedrosa de Jesus, J. D. *J. Phys. Chem. B* **1998**, *102*, 4739.

(8) Ghose, S.; Gupta, P. K. S.; Campana, C. F. *Can. Mineral.* **1987**, *72*, 365.

(9) Rocha, J.; Ferreira, P.; Carlos, L. D.; Ferreira, A. *Angew. Chem. Int. Ed.* **2000**, *39*, 3276.

(10) McGehee, M. D.; Bergstedt, T.; Zhang, C.; Saab, A. P.; O'Regan, M. B.; Bazan, G. C.; Srdanov, V. I.; Heeger, A. J. *Adv. Mater.* **1999**, *11*, 1349.

(11) Sá, G. F.; Malta., O. L.; Melo Donegá, C.; Simas, A. M.; Longo, R. L.; Santa Cruz, P. A.; Da Silva, E. F., Jr. *Coord. Chem. Rev.* **2000**, *196*, 165.

(12) Bünzli, J. C. G.; Choppin G. R., Eds. *Lanthanide Probes in Life, Chemical and Earth Sciences—Theory and Practice*; Elsevier: Amsterdam, 1989; Chapter 7.

(13) Carlos, L. D.; Messaddeq, Y.; Brito, H. F.; Sá Ferreira, R. A.; de Zea Bermudez, V.; Ribeiro, S. J. L. *Adv. Mater.* **2000**, *12*, 594

(14) Chen, J.; Selvin, P. R. *J. Photochem. Photobiol. A: Chem.* **2000**, *135*, 27.

(15) Serpaggi, F.; Luxbacher, I.; Cheetham, A. K.; Férey, G. *J. Solid State Chem.* **1999**, *145*, 580.

(16) Serpaggi, F.; Férey, G.; Antic-Fidancev, E. *J. Solid State Chem.* **1999**, *148*, 347.

10.1021/ja010244z CCC: $20.00
Published on Web 05/26/2001

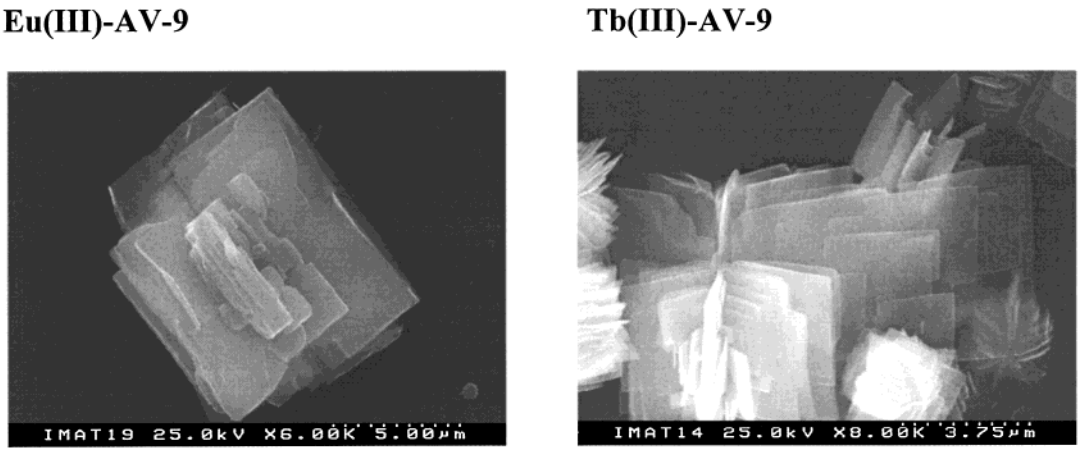

Figure 1. SEM images of Eu(III)- and Tb(III)-AV-9.

Table 1. Monoclinic Unit Cell Parameters and Details of of Rietveld Refinement

	$(K_1Na_2)EuSi_8O_{19}\cdot 5H_2O$	$(K_1Na_2)TbSi_8O_{19}\cdot 5H_2O$
cell parameters:		
a, Å	23.973(3)	23.945(3)
b, Å	14.040(2)	14.019(2)
c, Å	6.5655(8)	6.5542(7)
β, deg	90.352(2)	90.288(3)
volume, Å^3	2210.5(5)	2200.1(4)
space group	*C*2/*m*	*C*2/*m*
formula units/cell (*Z*)	4	4
formula mass, g	855.8	862.7
calcd density, g/cm^3	2.57	2.60
zero point	−0.053(3)	−0.040(3)
transparency correction	−0.08(1)	0.006(4)
profile parameters:		
pseudo-Voigt function [$PV = \eta L + (1 - \eta)G$]		
η	0.78(1)	0.96(2)
Caglioti law parameters		
U	0.026(9)	0.007(4)
V	0.019(6)	0.053(7)
W	0.0129(8)	0.0053(8)
symmetry parameters (up to 35° 2θ)	0.062(4)	0.055(5)
	0.0409(8)	0.0348(9)
no. of "independent" reflcns	1703	1703
no. of global refined parameters	8	8
no. of profile refined parameters	11	11
no. of intensity-dependent refined parameters	59	59
reliability factors		
R_B	4.93	7.00
R_F	3.61	3.88
cR_P	9.48	13.7
cR_{wp}	12.3	17.1
χ^2	5.53	8.58

structure named AV-9 and with composition $Na_4K_2X_2Si_{16}O_{38}\cdot 10H_2O$ (X = Eu, Tb). To the best of our knowledge, these are the first examples of europium and terbium silicates with zeolitic properties. Although the structures of montregianite and AV-9 solids are related, important differences exist, particularly in the constitution of the octahedral (Na, Y, Eu, Tb) layers.

Experimental Section

Syntheses. The synthesis of AV-9 materials were carried out in Teflon-lined autoclaves (45 cm^3 volume , filling rate 0.5), under static hydrothermal conditions, in ovens preheated at 230 °C. In all the syntheses, the autoclaves were removed and quenched in cold water after an appropriate time. The off-white microcrystalline powders were filtered, washed at room temperature with distilled water, and dried at 100 °C.

Typical Eu(III)-AV-9 Synthesis. An alkaline solution was made by mixing 3.13 g of sodium silicate solution (27% m/m SiO_2, 8% m/m Na_2O, Merck), 19.38 g of H_2O, 0.43 g of KOH (Merck), 0.13 g of KCl (Merck), and 0.46 g of NaCl (Panreac). $EuCl_3\cdot 6H_2O$ (0.50 g, Aldrich) was added to this solution, and the mixture was stirred thoroughly. The gel, with the composition 0.57 Na_2O:0.37 K_2O:1.0 SiO_2:0.05 Eu_2O_3:76 H_2O, was autoclaved under autogenous pressure for 6 days at 230 °C. The initial and final gel pH (measured after 1:100 water dilution) was 10.5 and 11.1, respectively.

Typical Tb(III)-AV-9 Synthesis. An alkaline solution was made by mixing 7.40 g of sodium silicate solution (27% m/m SiO_2, 8% m/m Na_2O, Merck), 19.16 g of H_2O, 0.69 g of KOH (Merck), and 0.58 g of NaCl (Panreac). $Tb(NO_3)_3\cdot 5H_2O$ (2.00 g, Aldrich) was added to this solution, and the mixture was stirred thoroughly. The gel, with composition 0.44 Na_2O:0.18 K_2O:1.0 SiO_2:0.07 Tb_2O_3:32.0 H_2O, was autoclaved under autogenous pressure for 6 days at 230 °C. The initial and final gel pH (measured after 1:100 water dilution) was 10.6 and 11.2, respectively.

Chemical analysis (EDS) yields: for Eu(III)-AV-9 Si:Eu:Na:K molar ratios of ca. 7.9:1:2.2:0.9, and for Tb(III)-AV-9 Si:Tb:Na:K molar ratios of ca. 8.0:1.0:1.8:0.7. Thermogravimetry reveals a total weight loss of ca. 10.5% between 30 and 280 °C in the two materials corresponding

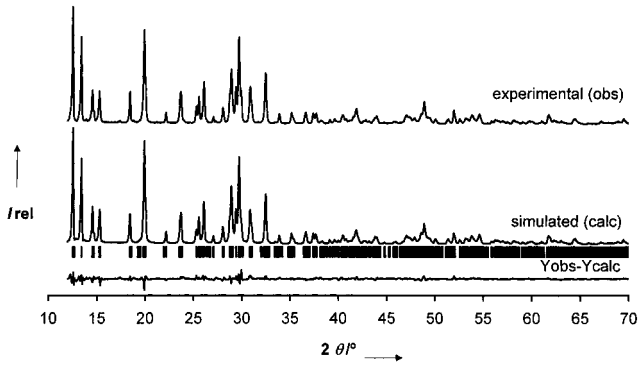

Figure 2. Observed, calculated, and difference powder XRD pattern of Eu(III)-AV-9.

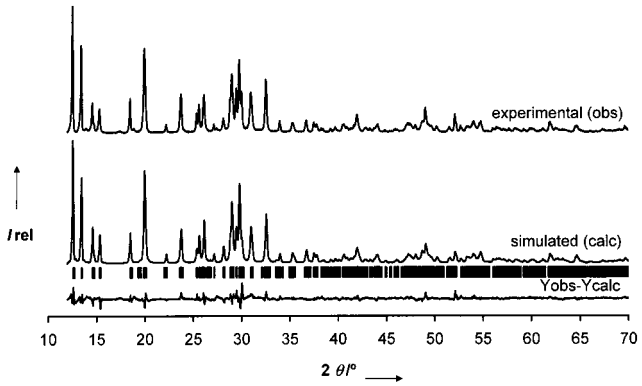

Figure 3. Observed, calculated, and difference powder XRD pattern of Tb(III)-AV-9.

Table 2. Fractional Atomic Coordinates and Isotropic Thermal Parameters for $(K_1Na_2)EuSi_8O_{19}\cdot 5H_2O$ (standard deviations are in parentheses)

name	*x*	*y*	*z*	B_{iso} (Å^2)	occupation
Eu1	1/2	0	0	1.70(9)	1/4
Eu2	0	0	0	1.70(9)	1/4
Si1	0.3869(4)	0.1384(8)	0.747(1)	1.4(1)	1
Si2	0.1132(6)	0	0.603(2)	1.4(1)	1/2
Si3	0.1126(4)	0.1346(7)	0.217(1)	1.4(1)	1
Si4	0.3197(5)	0	0.020(2)	1.4(1)	1/2
Si5	0.3882(4)	0	0.398(2)	1.4(1)	1/2
Si6	0.1867(5)	0	−0.011(2)	1.4(1)	1/2
K	1/4	1/4	0	6.8(3)	1/2
Na1	1/2	0.248(2)	0	3.4(3)	1/2
Na2	0	0.1240(9)	1/2	3.4(3)	1/2
O1	0.3913(8)	0.099(1)	0.514(2)	3.0(1)	1
O2	0.1590(7)	0.099(1)	0.062(2)	3.0(1)	1
O3	0.4383(7)	0	0.247(3)	3.0(1)	1/2
O4	0.2533(6)	0	0	3.0(1)	1/2
O5	0.0492(5)	0.123(1)	0.173(2)	3.0(1)	1
O6	0.3703(5)	0.2512(9)	0.744(2)	3.0(1)	1
O7	0.3357(9)	0	0.253(3)	3.0(1)	1/2
O8	0.3380(7)	0.085(1)	0.870(2)	3.0(1)	1
O9	0.0520(6)	0	0.697(2)	3.0(1)	1/2
O10	0.1684(9)	0	0.744(3)	3.0(1)	1/2
O11	0.4400(6)	0.125(1)	0.893(2)	3.0(1)	1
O12	0.1208(8)	0.087(1)	0.439(2)	3.0(1)	1
Ow1	0.4439(6)	0.264(2)	0.290(2)	6.5(4)	1
Ow2	0.3031(6)	0.242(4)	0.359(2)	6.5(4)	1
Ow3	1/2	0.152(2)	1/2	6.5(4)	1/2

to 5 water molecules per Eu(III) or Tb(III). N_2 adsorption isotherms of Eu(III)- and Tb(III)-AV-9 materials are of Type I (according to the IUPAC classification, $d < 2$ nm) characteristic of microporous solids with a negligible external surface area and maximum N_2 uptakes of 1.3 and 0.9 mmol·$g_{catalyst}^{-1}$. The Langmuir surface areas are 128.5 and 91.2 m^2 g^{-1} while the specific total pore volumes are 0.046 and 0.032 cm^3 g^{-1}, respectively. Powder XRD shows that the structure of AV-9 materials is stable up to 600 °C. SEM (Figure 1) shows that Eu(III)- and Tb(III)-AV-9 consist of microcrystalline thin plates.

Table 3. Main Interatomic Distances (Å) in $(K_1Na_2)EuSi_8O_{19}\cdot 5H_2O$

bond	distance	bond	distance	bond	distance
Eu(1)−O(3)	2.20(2)	Na(2)−O(5)	2.45(1)	Si(4)−O(4)	1.60(2)
Eu(1)−O(3)	2.20(2)	Na(2)−O(5)	2.45(1)	Si(4)−O(7)	1.57(2)
Eu(1)−O(11)	2.37(1)	Na(2)−O(9)	2.50(1)	Si(4)−O(8)	1.61(2)
Eu(1)−O(11)	2.37(1)	Na(2)−O(9)	2.50(1)	Si(4)−O(8)	1.61(2)
Eu(1)−O(11)	2.37(1)	Na(2)−Ow(1)	2.48(2)		
Eu(1)−O(11)	2.37(1)	Na(2)−Ow(1)	2.48(2)	Si(5)−O(1)	1.59(2)
				Si(5)−O(1)	1.59(2)
Eu(2)−O(5)	2.38(1)	Si(1)−O(1)	1.63(2)	Si(5)−O(3)	1.56(2)
Eu(2)−O(5)	2.38(1)	Si(1)−O(6)	1.63(2)	Si(5)−O(7)	1.57(2)
Eu(2)−O(5)	2.38(1)	Si(1)−O(8)	1.61(2)		
Eu(2)−O(5)	2.38(1)	Si(1)−O(11)	1.60(2)	Si(6)−O(2)	1.61(2)
Eu(2)−O(9)	2.35(2)			Si(6)−O(2)	1.61(2)
Eu(2)−O(9)	2.35(2)	Si(2)−O(9)	1.59(2)	Si(6)−O(4)	1.60(2)
		Si(2)−O(10)	1.61(2)	Si(6)−O(10)	1.66(2)
Na(1)−O(5)	2.44(2)	Si(2)−O(12)	1.64(2)		
Na(1)−O(5)	2.44(2)	Si(2)−O(12)	1.64(2)	K−O(2)	3.07(2)
Na(1)−O(11)	2.35(2)			K−O(2)	3.07(2)
Na(1)−O(11)	2.35(2)	Si(3)−O(2)	1.59(2)	K−O(6)	3.34(1)
Na(1)−Ow(1)	2.35(2)	Si(3)−O(5)	1.56(1)	K−O(6)	3.34(1)
Na(1)−Ow(1)	2.35(2)	Si(3)−O(6)	1.67(2)	K−O(8)	3.25(2)
		Si(3)−O(12)	1.61(2)	K−O(8)	3.25(2)
				K−Ow(2)	2.67(1)
				K−Ow(2)	2.67(1)

Table 4. Main Bond Angles (deg) in $(K_1Na_2)EuSi_8O_{19}\cdot 5H_2O$

bond	angle (deg)	bond	angle (deg)	bond	angle (deg)
O_3−Eu_1−O_3	180(2)	O_5−Na_1−O_5	84.1(9)	O_1−Si_1−O_6	110(1)
O_3−Eu_1−O_{11}	79.0(9)	O_5−Na_1−O_{11}	168(1)	O_1−Si_1−O_8	112(2)
O_3−Eu_1−O_{11}	101(1)	O_5−Na_1−O_{11}	97(1)	O_1−Si_1−O_{11}	117(2)
O_3−Eu_1−O_{11}	79.0(9)	O_5−Na_1−Ow_1	80.0(9)	O_6−Si_1−O_8	106(1)
O_3−Eu_1−O_{11}	101(1)	O_5−Na_1−Ow_1	92(1)	O_6−Si_1−O_{11}	108(1)
O_3−Eu_1−O_{11}	101(1)	O_5−Na_1−O_{11}	97(1)	O_8−Si_1−O_{11}	103(2)
O_3−Eu_1−O_{11}	79.0(9)	O_5−Na_1−O_{11}	168(1)		
O_3−Eu_1−O_{11}	101(1)	O_5−Na_1−Ow_1	92(1)	O_9−Si_2−O_{10}	122(2)
O_3−Eu_1−O_{11}	79.0(9)	O_5−Na_1−Ow_1	80.1(9)	O_9−Si_2−O_{12}	111(2)
O_{11}−Eu_1−O_{11}	84.5(8)	O_{11}−Na_1−O_{11}	86(1)	O_9−Si_2−O_{12}	111(2)
O_{11}−Eu_1−O_{11}	95.5(8)	O_{11}−Na_1−Ow_1	88(1)	O_{10}−Si_2−O_{12}	107(2)
O_{11}−Eu_1−O_{11}	180(1)	O_{11}−Na_1−Ow_1	100(1)	O_{10}−Si_2−O_{12}	107(2)
O_{11}−Eu_1−O_{11}	180(1)	O_{11}−Na_1−Ow_1	100(1)	O_{12}−Si_2−O_{12}	96(1)
O_{11}−Eu_1−O_{11}	95.5(8)	O_{11}−Na_1−Ow_1	88(1)		
O_{11}−Eu_1−O_{11}	84.5(8)	Ow_1−Na_1−Ow_1	169(1)	O_2−Si_3−O_5	122(2)
				O_2−Si_3−O_6	103(1)
O_5−Eu_2−O_5	86.8(7)	O_5−Na_2−O_5	179.3(9)	O_2−Si_3−O_{12}	111(2)
O_5−Eu_2−O_5	93.2(9)	O_5−Na_2−O_9	102.0(8)	O_5−Si_3−O_6	111(1)
O_5−Eu_2−O_5	180(1)	O_5−Na_2−O_9	77.5(7)	O_5−Si_3−O_{12}	104(1)
O_5−Eu_2−O_9	98.1(9)	O_5−Na_2−Ow_1	77.3(9)	O_6−Si_3−O_{12}	103(1)
O_5−Eu_2−O_9	81.9(7)	O_5−Na_2−Ow_1	103(1)		
O_5−Eu_2−O_5	180(1)	O_5−Na_2−O_9	77.5(7)	O_4−Si_4−O_7	109(2)
O_5−Eu_2−O_5	93.2(9)	O_5−Na_2−O_9	102.0(8)	O_4−Si_4−O_8	103(1)
O_5−Eu_2−O_9	81.9(8)	O_5−Na_2−Ow_1	103(1)	O_4−Si_4−O_8	103(1)
O_5−Eu_2−O_9	98.1(9)	O_5−Na_2−Ow_1	77.3(9)	O_7−Si_4−O_8	122(2)
O_5−Eu_2−O_5	86.8(7)	O_9−Na_2−O_9	91.7(9)	O_7−Si_4−O_8	122(2)
O_5−Eu_2−O_9	98.1(9)	O_9−Na_2−Ow_1	175(1)	O_8−Si_4−O_8	95(2)
O_5−Eu_2−O_9	81.9(8)	O_9−Na_2−Ow_1	84(1)		
O_5−Eu_2−O_9	81.9(8)	O_9−Na_2−Ow_1	84(1)	O_1−Si_5−O_1	122(2)
O_5−Eu_2−O_9	98.1(9)	O_9−Na_2−Ow_1	175(1)	O_1−Si_5−O_3	106(2)
O_9−Eu_2−O_9	180(1)	Ow_1−Na_2−Ow_1	101(1)	O_1−Si_5−O_7	109(2)
				O_1−Si_5−O_3	106(2)
				O_1−Si_5−O_7	109(2)
				O_3−Si_5−O_7	103(2)
				O_2−Si_6−O_2	118(1)
				O_2−Si_6−O_4	114(2)
				O_2−Si_6−O_{10}	100(2)
				O_2−Si_6−O_4	114(2)
				O_2−Si_6−O_{10}	100(2)
				O_4−Si_6−O_{10}	107(3)

Measurements. Powder X-ray diffraction (XRD) data were collected on a X'Pert MPD Philips difractometer (CuKα X-radiation) with a curved graphite monochromator, a fixed divergence slit of 0.5°, and a

Table 5. Fractional Atomic Coordinates and Isotropic Thermal Parameters for $(K_1Na_2)TbSi_8O_{19}\cdot 5H_2O$ (standard deviations are in parentheses)

name	*x*	*y*	*z*	B_{iso}(Å^2)	occupation
Tb1	1/2	0	0	0.70(9)	1/4
Tb2	0	0	0	0.70(9)	1/4
Si1	0.3902(3)	0.1380(5)	0.740(1)	0.6(1)	1
Si2	0.1109(4)	0	0.604(2)	0.6(1)	1/2
Si3	0.1150(3)	0.1336(5)	0.219(1)	0.6(1)	1
Si4	0.3203(4)	0	0.012(2)	0.6(1)	1/2
Si5	0.3853(4)	0	0.381(2)	0.6(1)	1/2
Si6	0.1881(4)	0	−0.004(2)	0.6(1)	1/2
K	1/4	1/4	0	7.8(4)	1/2
Na1	1/2	0.249(1)	0	2.4(3)	1/2
Na2	0	0.1258(9)	1/2	2.4(3)	1/2
O1	0.4003(9)	0.093(1)	0.511(2)	2.7(2)	1
O2	0.1555(8)	0.100(1)	0.030(2)	2.7(2)	1
O3	0.44248(7)	0	0.266(3)	2.7(2)	1/2
O4	0.2533(4)	0	0	2.7(2)	1/2
O5	0.0500(4)	0.121(1)	0.180(2)	2.7(2)	1
O6	0.3731(6)	0.2519(5)	0.748(2)	2.7(2)	1
O7	0.3290(8)	0	0.252(2)	2.7(2)	1/2
O8	0.3372(6)	0.082(1)	0.853(2)	2.7(2)	1
O9	0.0496(5)	0	0.690(2)	2.7(2)	1/2
O10	0.1650(9)	0	0.758(2)	2.7(2)	1/2
O11	0.4393(6)	0.1256(9)	0.918(3)	2.7(2)	1
O12	0.1198(8)	0.095(1)	0.458(2)	2.7(2)	1
Ow1	0.4424(6)	0.254(2)	0.2748(5)	3.3(5)	1
Ow2	0.3007(5)	0.229(2)	0.377(3)	3.3(5)	1
Ow3	1/2	0.155(2)	1/2	3.3(5)	1/2

Table 6. Main Interatomic Distances (Å) in $(K_1Na_2)TbSi_8O_{19}\cdot 5H_2O$

bond	distance	bond	distance	bond	distance
Tb(1)−O(3)	2.23(2)	Na(2)−O(5)	2.42(1)	Si(4)−O(4)	1.60(2)
Tb(1)−O(3)	2.23(2)	Na(2)−O(5)	2.42(1)	Si(4)−O(7)	1.59(2)
Tb(1)−O(11)	2.34(1)	Na(2)−O(9)	2.46(1)	Si(4)−O(8)	1.61(2)
Tb(1)−O(11)	2.34(1)	Na(2)−O(9)	2.46(1)	Si(4)−O(8)	1.61(2)
Tb(1)−O(11)	2.34(1)	Na(2)−Ow(1)	2.63(2)		
Tb(1)−O(11)	2.34(1)	Na(2)−Ow(1)	2.63(2)	Si(5)−O(1)	1.60(2)
				Si(5)−O(1)	1.60(2)
Tb(2)−O(5)	2.38(1)	Si(1)−O(1)	1.65(2)	Si(5)−O(3)	1.56(2)
Tb(2)−O(5)	2.38(1)	Si(1)−O(6)	1.65(1)	Si(5)−O(7)	1.59(2)
Tb(2)−O(5)	2.38(1)	Si(1)−O(8)	1.66(2)		
Tb(2)−O(5)	2.38(1)	Si(1)−O(11)	1.66(2)	Si(6)−O(2)	1.62(2)
Tb(2)−O(9)	2.36(1)			Si(6)−O(2)	1.62(2)
Tb(2)−O(9)	2.36(1)	Si(2)−O(9)	1.58(2)	Si(6)−O(4)	1.56(2)
		Si(2)−O(10)	1.64(2)	Si(6)−O(10)	1.65(2)
Na(1)−O(5)	2.47(2)	Si(2)−O(12)	1.65(2)		
Na(1)−O(5)	2.47(2)	Si(2)−O(12)	1.65(2)	K−O(2)	3.09(2)
Na(1)−O(11)	2.32(2)			K−O(2)	3.09(2)
Na(1)−O(11)	2.32(2)	Si(3)−O(2)	1.64(2)	K−O(6)	3.39(2)
Na(1)−Ow(1)	2.28(1)	Si(3)−O(5)	1.59(1)	K−O(6)	3.39(2)
Na(1)−Ow(1)	2.28(1)	Si(3)−O(6)	1.65(1)	K−O(8)	3.29(2)
		Si(3)−O(12)	1.66(1)	K−O(8)	3.29(2)
				K−Ow(2)	2.76(2)
				K−Ow(2)	2.76(2)

flat plate sample holder, in a Bragg−Brentano para-focusing optics configuration. Intensity data were collected by the step counting method (step 0.02° and time 10 s) in the range 2θ 6−110°. Powder XRD pattern autoindexing was performed with the Powder-X package from the well-resolved first 30 lines.[17] SEM images were recorded on a Hitachi S-4100 microscope. EDS was carried out using a EDS Römteck System with polymeric window attached to the scanning electron microscope. Thermogravimetric (TGA) curves were measured with a Mettler TG50 Thermobalance. The samples were heated under air at a rate of 5 °C/min. Nitrogen adsorption isotherms were measured at 77 K, using a gravimetric adsorption apparatus equipped with a CI electronic MK2-M5 microbalance and an Edwards Barocel pressure sensor. The solids were outgassed at 300 °C overnight to a residual pressure of ca. 10^{-4} mbar. Langmuir surface area was calculated assuming the projection area of the nitrogen molecule to be 0.162 nm^2/molecule. The specific total pore volumes were estimated from the N_2 uptake at P/P_0 ca. 0.95, using the liquid density of N_2 at 77 K, 0.8081 g cm^{-3}.

(17) Dong, C.; Wu, F.; Chen, H. *J. Appl. Crystallogr.* **1999**, *32*, 168.

Table 7. Main Bond Angles (deg) in $(K_1Na_2)TbSi_8O_{19}\cdot 5H_2O$

bond	angle (deg)	bond	angle (deg)	bond	angle (deg)
O_3−Tb1−O_3	180(2)	O_5−Na_1−O_5	85.3(8)	O_1−Si_1−O_6	115(1)
O_3−Tb1−O_{11}	78(1)	O_5−Na_1−O_{11}	164(1)	O_1−Si_1−O_8	109(1)
O_3−Tb1−O_{11}	102(1)	O_5−Na_1−O_{11}	98(1)	O_1−Si_1−O_{11}	119(2)
O_3−Tb1−O_{11}	78(1)	O_5−Na_1−Ow_1	84.1(9)	O_6−Si_1−O_8	105(1)
O_3−Tb1−O_{11}	102(1)	O_5−Na_1−Ow_1	93.6(9)	O_6−Si_1−O_{11}	105(1)
O_3−Tb1−O_{11}	102(1)	O_5−Na_1−O_{11}	98(1)	O_8−Si_1−O_{11}	100(1)
O_3−Tb1−O_{11}	78(1)	O_5−Na_1−O_{11}	164(1)		
O_3−Tb1−O_{11}	102(1)	O_5−Na_1−Ow_1	93.6(9)	O_9−Si_2−O_{10}	121(2)
O_3−Tb1−O_{11}	78(1)	O_5−Na_1−Ow_1	84.1(9)	O_9−Si_2−O_{12}	109(1)
O_{11}−Tb1−O_{11}	82.6(8)	O_{11}−Na_1−O_{11}	84(1)	O_9−Si_2−O_{12}	109(1)
O_{11}−Tb1−O_{11}	97.4(8)	O_{11}−Na_1−Ow_1	79.9(9)	O_{10}−Si_2−O_{12}	105(1)
O_{11}−Tb1−O_{11}	180(1)	O_{11}−Na_1−Ow_1	103(1)	O_{10}−Si_2−O_{12}	105(1)
O_{11}−Tb1−O_{11}	180(1)	O_{11}−Na_1−Ow_1	103(1)	O_{12}−Si_2−O_{12}	107(2)
O_{11}−Tb1−O_{11}	97.4(8)	O_{11}−Na_1−Ow_1	79.9(9)		
O_{11}−Tb1−O_{11}	82.6(8)	Ow_1−Na_1−Ow_1	176.9(8)	O_2−Si_3−O_5	115(1)
				O_2−Si_3−O_6	106(1)
O_5−Tb2−O_5	89.2(7)	O_5−Na_2−O_5	176.8(9)	O_2−Si_3−O_{12}	125(1)
O_5−Tb2−O_5	90(1)	O_5−Na_2−O_9	100.3(8)	O_5−Si_3−O_6	107(1)
O_5−Tb2−O_5	180(1)	O_5−Na_2−O_9	77.4(6)	O_5−Si_3−O_{12}	100(1)
O_5−Tb2−O_9	99.9(9)	O_5−Na_2−Ow_1	78.0(8)	O_6−Si_3−O_{12}	100(1)
O_5−Tb2−O_9	80.1(7)	O_5−Na_2−Ow_1	104.1(8)		
O_5−Tb2−O_5	180(1)	O_5−Na_2−O_9	77.4(6)	O_4−Si_4−O_7	100(1)
O_5−Tb2−O_5	91(1)	O_5−Na_2−O_9	100.3(8)	O_4−Si_4−O_8	103(1)
O_5−Tb2−O_9	80.1(7)	O_5−Na_2−Ow_1	104.1(8)	O_4−Si_4−O_8	103(1)
O_5−Tb2−O_9	99.9(9)	O_5−Na_2−Ow_1	78.0(8)	O_7−Si_4−O_8	127(2)
O_5−Tb2−O_5	89.2(7)	O_9−Na_2−O_9	88.5(8)	O_7−Si_4−O_8	127(2)
O_5−Tb2−O_9	99.9(9)	O_9−Na_2−Ow_1	174(1)	O_8−Si_4−O_8	92(1)
O_5−Tb2−O_9	80.1(7)	O_9−Na_2−Ow_1	85.7(9)		
O_5−Tb2−O_9	80.1(7)	O_9−Na_2−Ow_1	85.7(9)	O_1−Si_5−O_1	109(2)
O_5−Tb2−O_9	99.9(9)	O_9−Na_2−Ow_1	174(1)	O_1−Si_5−O_3	94(2)
O_9−Tb2−O_9	180(1)	Ow_1−Na_2−Ow_1	100.1(8)	O_1−Si_5−O_7	118(2)
				O_1−Si_5−O_3	94(2)
				O_1−Si_5−O_7	118(2)
				O_3−Si_5−O_7	119(2)
				O_2−Si_6−O_2	120(1)
				O_2−Si_6−O_4	119(1)
				O_2−Si_6−O_{10}	88(1)
				O_2−Si_6−O_4	119(1)
				O_2−Si_6−O_{10}	88(1)
				O_4−Si_6−O_{10}	111(2)

The single-quantum ^{23}Na MAS NMR spectrum was measured using short and powerful radio frequency pulses (0.5 μs, equivalent to a 15° pulse angle), a spinning rate of 31.3 kHz, and a recycle delay of 1.5 s. Chemical shifts are quoted in ppm from 1 M aqueous NaCl. The triple-quantum ^{23}Na MAS NMR spectrum was recorded using a two-pulse sequence.[18] The lengths of the first and second hard pulses (radio frequency magnetic field amplitude v_1 = 160 kHz) were 4.3 and 1.3 μs, respectively. The MAS rate was v_R = 16 kHz. Thirty-four data points were acquired in the t_1 dimension in increments of $1/v_R$ = 62.5 μs (960 scans per spectrum). The ppm scale of the sheared spectrum was referenced to v_o frequency in the v_2 domain and to 3.78 v_o in the v_1 domain (reference 1 M aqueous NaCl).

The photoluminescence spectra were recorded on a 1 m Czerny-Turner spectrometer (1704 Spex), fitted with a 1200 grooves/mm grating blazed at 500 nm, coupled to a R928 Hamamatsu photomultiplier. A 300 W Xe arc lamp coupled to a 0.25 m excitation monochromator (Kratos GM-252) fitted with a 1180 grooves/mm grating blazed at 240 nm was used as the excitation source. All the spectra were corrected for the response of the detectors. The time-resolved measurements were carried out using a pulsed Xe arc lamp (5 mJ/pulse, 3 ms bandwidth) coupled to the monochromator Kratos GM-252 and a Spex 1934 C phosphorimeter.

Results and Discussion

Power XRD. A Eu(III)-AV-9 monoclinic unit cell, a = 11.989 Å, b = 7.020 Å, c = 6.568 Å, β = 90.377°, was

(18) Fernandez, C.; Amoureux, J.-P.; Chezeau, J. M.; Delmotte, L.; Kessler, H. *Microporous Mater.* **1996**, *6*, 331.

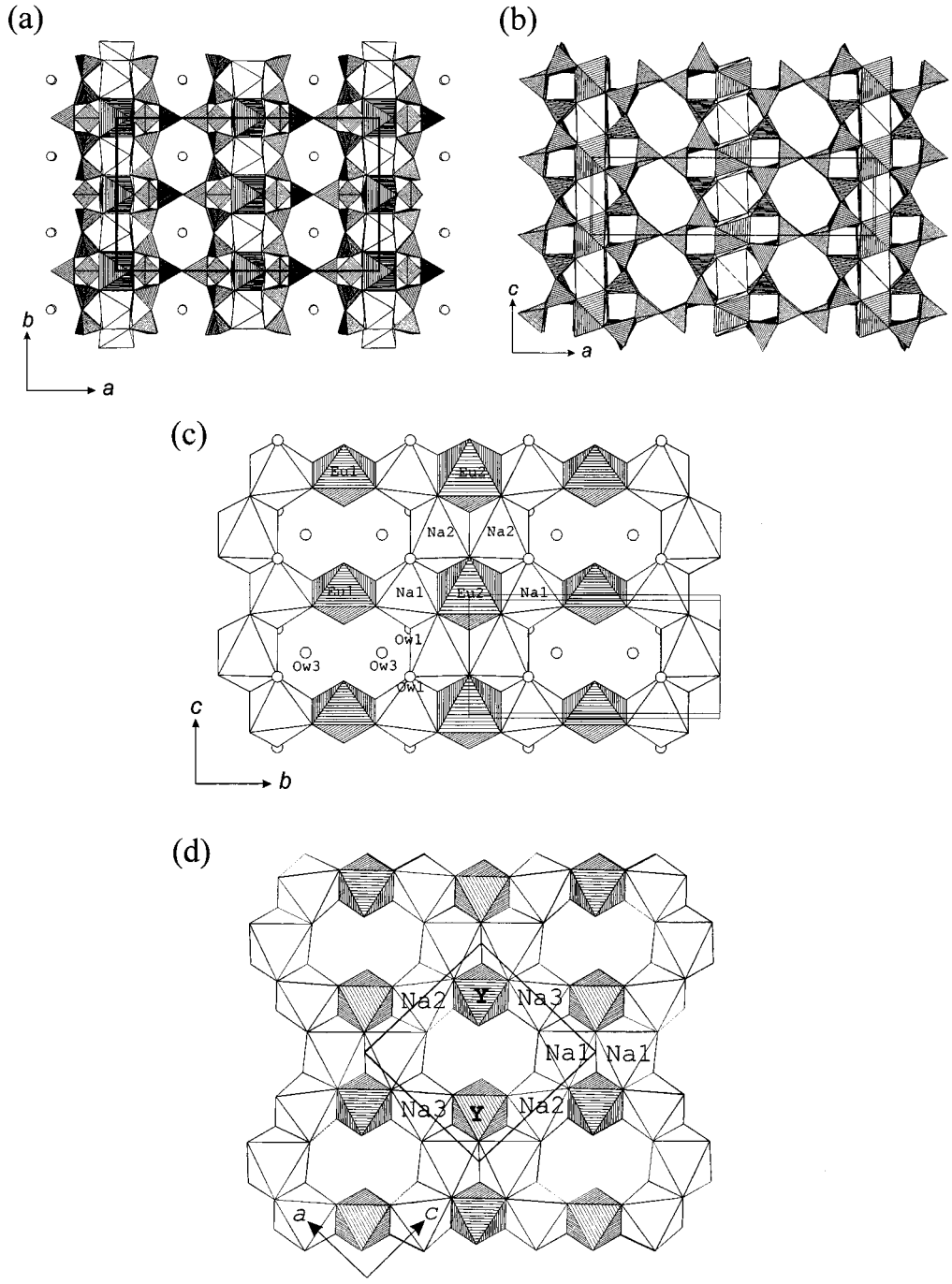

Figure 4. Schematic views of the structure of Eu(III)- and Tb(III)-AV-9. (a) Note the alternating octahedral sheet and double-silicate layer. (b) Channels along the *b* axis are defined by eight-membered rings and are free from any cations. Notice that the octahedral sheets of (c) AV-9 materials and (d) montregianite mineral are somewhat different (the layers have been cut away and *do not* represent projections down the *a* and *b* axes).

indicated by the TREOR90 indexing program[19] with high figures of merit, $M_{30} = 42$ and $F_{30} = 95$. This result was also confirmed with DICVOL.[20]

Luminescence spectroscopy indicated that the local Eu(III) symmetry was C_{2h} implying that the monoclinic cell belongs to a 2/*m* point group (see section on photoluminescence). With this information, two possible space groups were determined from the analysis of the systematic extinctions: *P*2/*m* and *C*2/*m* ($a' = 2a$, $b' = 2b$). These space groups were used to determine the crystal structure.

The ab initio crystal structure determination from powder XRD data was carried out with the package EXPO.[21] First, the structure factor amplitudes were extracted by the Le Bail method from the powder pattern.[22] Then, the structures were solved by direct methods. Although all atoms were located simultaneously, re-labeling of atoms was necessary as suggested by bond distances and bond angles. This procedure was alternated with least-squares refinements. The two trial structures are very

(19) Werner, P. E.; Eriksson L.; Westdahl, M. *J. Appl. Crystallogr.* **1985**, *18*, 367.
(20) Boultif, A.; Louër, D. *J. Appl. Crystallogr.* **1991**, *24*, 987.
(21) Altomare, A.; Burla, M. C.; Carmalli, M.; Carrozzini, B.; Cascarano, G. L.; Giacovazzo, C.; Guagliardi, A.; Moliterni, A.; Polidori G.; Rizzi, R. *J. Appl. Crystallogr.* **1999**, *32*, 339.
(22) Le Bail, A.; Duroy, H.; Fourquet, J. L. *Math. Res. Bull.* **1988**, *23*, 447.

similar; the structure with space group *P*2/*m* calls for the presence of a single Eu(III) site, while the *C*2/*m* structure possesses two nonequivalent Eu(III) sites. Luminescence spectroscopy suggested the presence of two Eu(III) sites. In addition, the *C*2/*m* structure *R* factor is lower than the *P*2/*m* structure factor, respectively 4.8 and 7.6%. Rietveld refinement was, thus, carried out in space group *C*2/*m*.

The coordinates of atoms obtained from direct methods were used in the Rietveld refinement of the structure by the FullProf program.[23] The final profile analysis refinement was carried out in the range 12−110° 2θ for the occurring 1703 independent reflections and involved the following parameters: 53 fractional atomic coordinates, 6 isotropic temperature factors, 1 scale factor, 1 parameter (η) for the pseudo-Voigt peak shape function, 3 parameters (*U, V, W*) to describe the angular dependence of the peak full-width at half-maximum, 4 unit cell parameters, 2 peak asymmetry parameters, 1 zero-point shift, 1 parameter for the transparency correction, and 6 coefficients of polynomial background. Several soft constraints to some of the bond distances were applied.

Since the powder XRD patterns of Eu(III)-AV-9 and Tb(III)-AV-9 are very similar, the structure of the latter was Rietveld refined using the structure of the former as a starting model. The final profile fits of Eu(III)-AV-9 and Tb(III)-AV-9 are shown in Figures 2 and 3 while Table 1 gives crystallographic data. The atomic coordinates are given in Tables 2 and 5, and bond distances and angles are collected in Tables 3, 6 and 4, 7, respectively.

The structure of Eu(III)- and Tb(III)-AV-9 consists of two different types of layers alternating along the [100] direction (Figure 4a): (a) a double silicate sheet, where the single silicate sheet is of the apophyllite type with four- and eight-membered rings, and (b) an open octahedral sheet, composed of two nonequivalent [EuO_6] octahedra and two distinct [$NaO_4(H_2O)_2$] octahedra (Figure 4c). The K^+ ions and the water molecules are located within large channels formed by the planar eight-membered silicate rings. The tetrahedral layers of AV-9 solids and montregianite are similar, but this is not the case with the octahedral layers (compare panels c and d in Figure 4). As far as luminescence properties are concerned, the most important difference between the octahedral layers of AV-9 and montregianite lies in the fact that the latter contains a single kind of Y(III), facing the pores, while AV-9 contains two kinds of Eu(III), Tb(III): one is isolated by [$NaO_4(H_2O)_2$] octahedra while the other is facing the pores. This is expected to influence the luminescence behavior of these two Eu(III), Tb(III) centers.

Solid-State NMR. Due to the strong interaction between the ^{23}Na nuclei and the paramagnetic Eu(III) centers, the "normal" (single-quantum) ^{23}Na magic-angle spinning (MAS) NMR spectrum of AV-9 displays a peak (with a shoulder) centered at 2 ppm with a strong spinning sideband manifold, ranging from 800 to −600 ppm (Figure 5). The triple-quantum ^{23}Na MAS NMR spectrum (Figure 6) reveals the presence of two peaks, thus supporting the proposed Eu-AV-9 structure. This material displays a complex ^{29}Si MAS NMR spectrum (not shown) with a strong spinning sideband pattern ranging from ca. 120 to −550 ppm. The main resonance is centered at −100.2 ppm. At least two other much fainter peaks are observed at −131.6 and −244.1 ppm. These resonances experience a low-frequency shift induced by paramagnetic Eu(III). Synthetic yttrium montregianite displays a different spectrum but it does not contain any paramagnetic centers.[6,7] It is, thus, difficult to draw any conclusions on the structure of AV-9 based on the ^{29}Si MAS NMR evidence. Due to the strong paramagnetism of the Tb(III) ion which renders the resonances too broad to be detected, no ^{23}Na or ^{29}Si NMR spectra could be recorded for Tb(III)-AM-9.

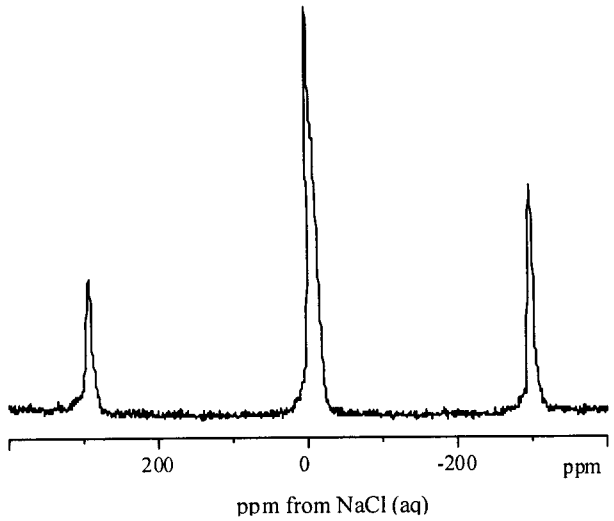

Figure 5. Selected region of the single-quantum ('normal') ^{23}Na MAS NMR spectrum of Eu(III)-AV-9.

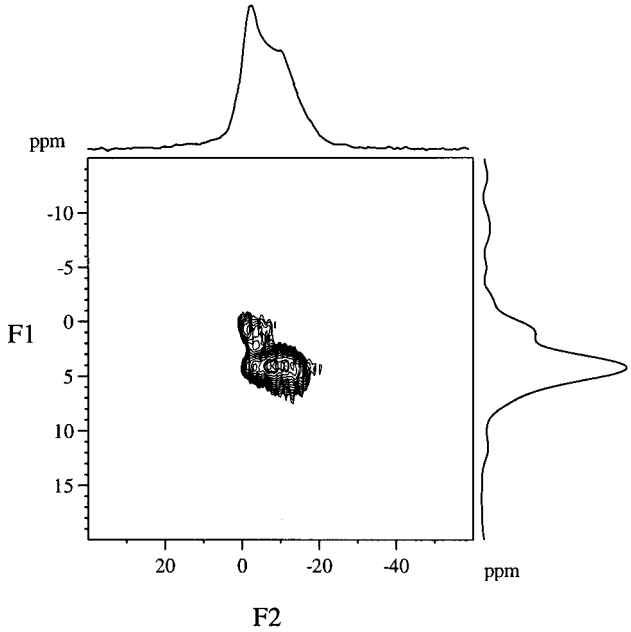

Figure 6. Triple-quantum ^{23}Na MAS NMR spectrum of Eu(III)-AV-9.

Photoluminescence. Figure 7 shows the room-temperature emission spectra of Eu(III)-AV-9. The inset displays the corresponding excitation spectrum. The sharp emission lines are assigned to transitions between the first excited nondegenerate $^5D_0$ state and the $^7F_{0-4}$ levels of the fundamental Eu(III) septet. Luminescence from higher excited states such as $^5D_1$ is not detected, indicating very efficient nonradiative relaxation to the $^5D_0$ level. Except for the $^5D_0 \rightarrow {}^7F_1$ lines, which have a predominant magnetic dipole character, the observed transitions are mainly of electric dipole nature. The excitation lines are assigned to the $^7F_{0-1} \rightarrow {}^5D_{4-1}$, $^5L_6$, and ^5G_J transitions. The changes detected on the $^5D_0 \rightarrow {}^7F_{0,2}$ transitions as the excitation wavelength varies from 394 ($^5L_6$) to 527 nm ($^5D_1$), namely in the $^5D_0 \rightarrow {}^7F_0$ full width at half-maximum and in relative intensity of the $^7F_2$ Stark levels (Figure 8), clearly suggest the presence of two distinct Eu(III) environments. This is unequivo-

(23) Rodriguez-Carvajal, J. *Collected Abstracts of Powder Diffraction Meeting*; Toulouse, France, July 1990; p 127.

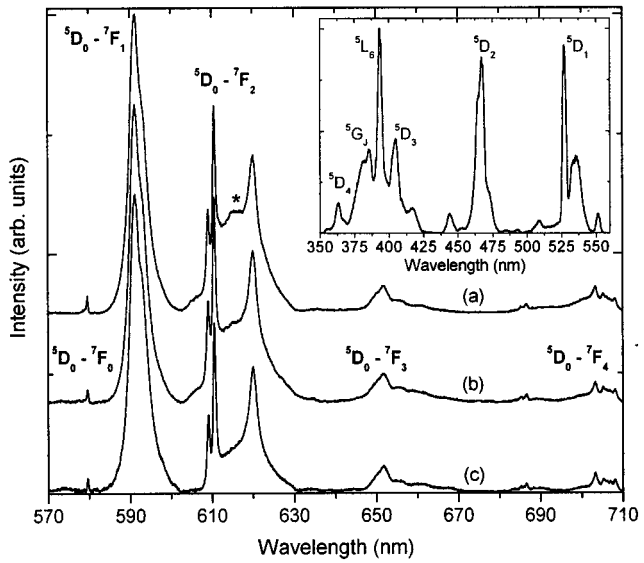

Figure 7. Emission spectra of Eu(III)-AV-9 (300 K) excited at three different wavelengths: (a) 394, (b) 466, and (c) 527 nm. For clarity, the spectra are vertically shifted with respect to each other. The inset shows the room-temperature excitation spectrum detected within the $^7F_1$ manifold (591.5 nm).

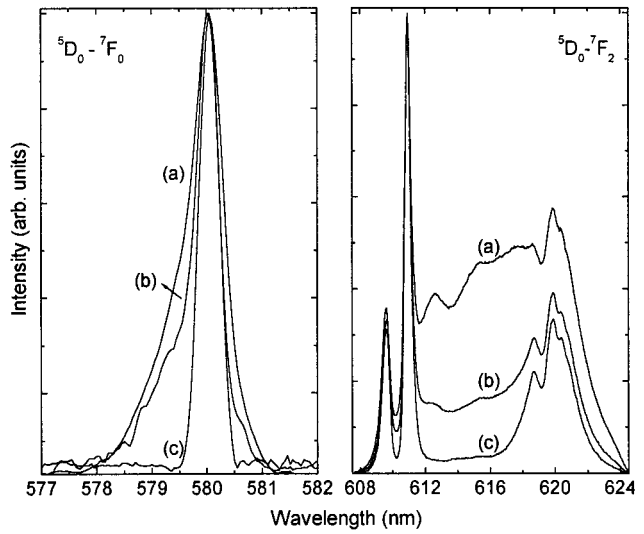

Figure 8. The emission $^5D_0 \rightarrow {}^7F_0$ and $^5D_0 \rightarrow {}^7F_2$ transitions of Eu^{3+} AV-9 (45 K) excited at (a) 394, (b) 466, and (c) 527 nm.

cally confirmed by the analysis of the $^5D_0$ decay curves illustrated in Figure 9. For an excitation of 527 nm the $^5D_0$ decay curve recorded at the strongest $^7F_1$ level is well fitted by a single exponential, indicating an Eu(III) site with a lifetime around 3.50 ± 0.01 ms. However, for a 394 nm excitation a biexponential behavior is clearly observed and a shorter lifetime (0.75 ± 0.01 ms) was measured in the $^7F_2$ region (depicted with an asterisk in Figure 7). While a lifetime of 3.50 ms is typical of anhydrous inorganic Eu(III) crystals, a 0.75 ms lifetime may indicate the coordination of water molecules or hydroxyl groups to Eu(III).[12] However, according to the powder XRD structure no such Eu environments are present in Eu(III)-AV-9. To better understand this problem, a preliminary time-resolved photoluminescence study of an Eu(III)-AV-9 sample dehydrated in a vacuum at 400 °C for 12 h was carried out. It was found that the fast $^5D_0$ component lifetime remained unchanged, thus showing that the corresponding Eu(III) is not coordinated by water or hydroxyls and supporting the proposed powder XRD structure.

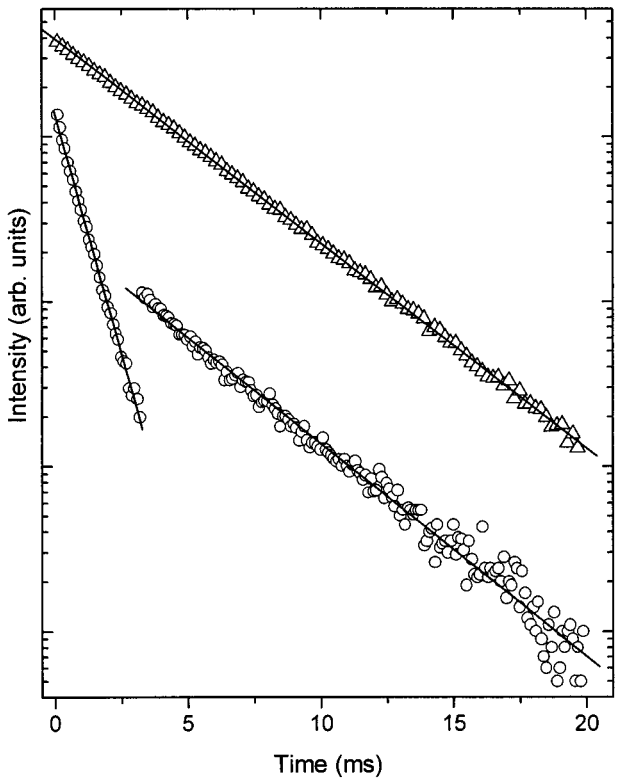

Figure 9. Room-temperature $^5D_0$ decay curves for Eu(III)-AV-9 detected at the strongest $^7F_1$ Stark level (triangles) and within the $^7F_2$ manifold (circles), excited at 394 and 527 nm, respectively. The straight lines represent the best fits ($r^2 = 0.99$) to the data considering a single and a biexponential behavior, respectively.

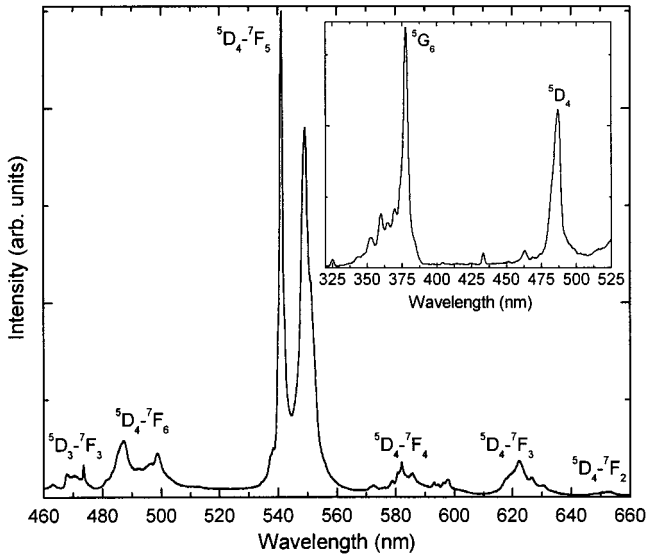

Figure 10. Emission spectrum of Tb(III)-AV-9 (300 K) excited at 378 nm. The inset shows the room-temperature excitation spectrum detected at 541 nm ($^7F_5$ manifold).

The $^5D_0 \rightarrow {}^7F_1$ magnetic transition is stronger than the $^5D_0 \rightarrow {}^7F_2$ forced electric-dipole one for both two Eu(III) local environments. This indicates that the local symmetry of the corresponding Eu(III) sites has an inversion center.[12,24] Moreover, the observed splitting of the $^7F_{1-2}$ levels and the existence of an inversion center indicate that the point symmetry group of the AV-9 lanthanide ions may be *C*2*h*,[19] consistent with the montregianite space group *C*2/*m* mentioned above.

(24) Carlos, L. D.; Videira, A. L. L. *Phys. Rev. B* **1994**, *49*, 11721.

Figure 10 shows the room-temperature emission and excitation spectra of Tb(III)-AV-9. The emission lines are assigned to the $^5D_{4,3} \rightarrow {}^7F_J$ ($J = 2-6$) transitions, while the $^7F_6 \rightarrow {}^5G_6$, $^5D_4$ lines dominate the excitation spectrum (inset in Figure 10). For Tb(III)-AV-9 the number of distinct $^7F_{2-6}$ Stark components and their intensity variation with the excitation wavelength do not allow the identification of more than one local site metal environment. However, this presence is clearly inferred by the analysis of the corresponding $^5D_4$ decay curves, excited at 486 nm and detected at the strongest $^5D_4 \rightarrow {}^7F_5$ transition line. The curves (not shown) are well fitted by biexponential functions resulting in experimental lifetimes around 8.67 ± 0.04 and 1.85 ± 0.07 ms.

In conclusion, the synthesis and characterization of the first microporous europium(III) and terbium(III) silicates have been reported. Because K^+ ions reside in the micropores, AV-9 materials may exhibit ion-exchange properties. If so, AV-9 materials have the potential to combine microporosity, ion-exchange, and luminescence properties.

Acknowledgment. This work was supported by PRAXIS XXI, FCT, POCTI, and FEDER. We thank Dr. A. Valente for recording the N_2 adsorption isotherms.

Supporting Information Available: X-ray crystallographic files (CIF). This material is available free of charge via the Internet at http://pubs.acs.org.

JA010244Z